Acousto-elasticity of transversely isotropic incompressible soft tissues: characterization of skeletal striated muscle

Jean-Pierre Remeniéras, Mahé Bulot, Jean-Luc Gennisson, Frédéric Patat, Michel Destrade, Guillaume Bacle

Acousto-elasticity of Transversely Isotropic Incompressible Soft Tissues: Characterization of Skeletal Striated Muscle

Jean-Pierre Remeniéras[1*], Mahé Bulot[1], Jean-Luc Gennisson[2], Frédéric Patat[1,3], Michel Destrade[4] and Guillaume Bacle[1,5]

[1]UMR 1253, iBrain, Université de Tours, Inserm, Tours, France.
[2]Laboratoire d'imagerie biomédicale multimodale à Paris-Saclay, Université Paris-Saclay, CEA, CNRS UMR 9011, INSERM UMR 1281, France.
[3]Inserm CIC-IT 1415, Tours, France.
[4]School of Mathematics, Statistics and Applied Mathematics, NUI Galway, University Road, Galway, Ireland.
[5]Service de chirurgie orthopédique 1A, Unité de chirurgie de la main et du membre supérieur, CHRU de Tours

E-mail: `jean-pierre.remenieras@univ-tours.fr`

Abstract.

Using shear wave elastography, we measure the changes in the wave speed with the stress produced by a striated muscle during isometric voluntary contraction. To isolate the behaviour of an individual muscle from complementary or antagonistic actions of adjacent muscles, we select the *flexor digiti minimi* muscle, whose sole function is to extend the little finger. To link the wave speed to the stiffness, we develop an acousto-elastic theory for shear waves in homogeneous, transversely isotropic, incompressible solids subject to an uniaxial stress. We then provide measurements of the apparent shear elastic modulus along, and transversely to, the fibre axis for six healthy human volunteers of different age and sex. The results display a great variety across the six subjects. We find that the slope of the apparent shear elastic modulus along the fibre direction changes inversely to the maximum voluntary contraction (MVC) produced by the volunteer. We propose an interpretation of our results by introducing the S (slow) or F (fast) nature of the fibres, which harden the muscle differently and accordingly, produce different MVCs. This work opens the way to measuring the elastic stiffness of muscles in patients with musculoskeletal disorders or neurodegenerative diseases.

Keywords: Acousto-elasticity, Shear Wave Elastography, Transversely Isotropic soft solid, Third order elastic constants, Musculoskeletal disorders, Maximum Voluntary Contraction.

Submitted to: *Phys. Med. Biol.*

1. Introduction

Affecting around 25% of people worldwide, musculoskeletal disorders have a high prevalence in the adult population, coupled to enormous and increasing health and societal impacts (Adams and Marano, 1995; Woolf and Åkesson, 2001; WHO ScientificGroup, 2003; Badley et al., 1994). Although mainly non-lethal, these pathologies cause significant morbidity with decreased function in daily life activities and lower quality of life (Vos et al., 2012; Reginster and Khaltaev, 2002; Storheim and Zwart, 2014). They also generate significant economic costs (Jacobson et al., 1996; WHO ScientificGroup, 2003).

The pathophysiology of many of these disorders is still not completely understood and the development of new diagnostic strategies and bio-markers specific to musculoskeletal tissues is crucial to medical progress (Storheim and Zwart, 2014). Also, skeletal, voluntary-controlled, muscles play a big role in motorizing joints, maintaining posture, and regulating peripheral blood flow. Hence, innovative assessments of muscle mechanical properties and dynamics linked to its very specific structural fibrillary organization can improve our understanding of normal and pathological muscle tissue behaviour and strength (Gijsbertse et al., 2017; Storheim and Zwart, 2014).

Over the past twenty years, ultrasound imaging techniques have gained sufficient temporal resolution to became ultra-fast (>1000 frames/s) and investigate the kinematics of muscle. Hence, they have been used to assess the dynamical behaviour and structural changes of normal and pathological contractile tissues (Deffieux et al., 2008a; Downs et al., 2018; Eranki et al., 2013; Lopata et al., 2010; Loram et al., 2006; Dhooge et al., 2000; Yeung et al., 1998; Miyatake et al., 1995; Nagueh et al., 1998).

Nonetheless, the biomechanical characteristics of skeletal muscle remain difficult to clarify fully because of its complex structural organization and its contractile properties (Gennisson et al., 2010). Indeed, as can be seen to the naked eye, skeletal muscle tissue is composed of families of parallel muscular fibres. Muscle contraction is carried out by the shortening of these fibres, which results from the active sliding of the thick myosin filaments between the fine actin filaments found within the fibres. Therefore, the main biomechanical characteristics of muscle tissue associated with contraction are shortening and hardening (Ford et al., 1981). Thus, techniques that provide quantitative data on tissue deformation and elastic properties could be of great help in understanding dynamic muscle behaviour. One such technique is quantitative Shear Wave Elastography (SWE), proposed by Sarvazyan et al. (1998), and then refined and used to quantitatively characterize the mechanical parameters of normal skeletal muscle tissues (Gennisson et al., 2010; Bouillard et al., 2011; Koo et al., 2014; Nordez et al., 2008; Nordez and Hug, 2010; Tran et al., 2016). Some attempts have also been made to indirectly evaluate muscle forces based on muscle elasticity using SWE (Bouillard et al., 2011; Kim et al., 2018; Hug et al., 2015).

Interestingly, muscle stiffness increases differently with tension during sustained contraction, depending on the type of motor units activated, according to Petit et al.

(1990), who performed measurements in the *peroneus longus* muscle of anesthetized cats. These authors found that the stiffness/tension slope is greater when (slow) S-type motor units are activated, compared to (fast fatigue-resistant) FR-type and (fast fatiguable) FF-type motor units. Their result suggests that S-type motor units contribute more to muscle hardness during contraction than F-type ones, and that the stiffness/tension relationship must consequently change according to the S/F ratio.

During voluntary contraction, an axial stress is induced inside the muscle tissue by the shortening of the fibres which modifies its mechanical properties. The goal of this paper is to measure experimentally the changes in shear wave speed during voluntary contraction on healthy volunteers and to model these changes with the acousto-elasticity (AE) theory. This theory is based on non linear elasticity of materials which links the speed of mechanical waves to uni-axial stress using high order elastic constants. Due to the presence of fibres, muscles are considered as anisotropic, specifically transverse isotropic (TI). It follows that shear waves propagate at different speeds depending on the orientation of the propagation and polarization directions with respect to the fibre axis (Gennisson et al., 2003). We show in first section how the AE theory can be adapted to study shear wave propagation in an homogeneous TI incompressible solid, subject to a uniaxial stress, extending the available theory for isotropic solids (Gennisson et al., 2007; Destrade et al., 2010b). Acousto-elasticity theory links the shear wave speed to the uniaxial stress (Gennisson et al., 2007) or, equivalently, to the uni-axial elongation (Destrade et al., 2010b). Both formulations have been used for *in vivo* experiments when the stress is applied directly by pressing the ultrasound probe onto the tissue (Latorre-Ossa et al., 2012; Jiang et al., 2015; Bernal et al., 2015; Otesteanu et al., 2019; Bayat et al., 2019). These approach was also developed to TI media (Bied et al., 2020). Here we measured the stress directly with a force sensor (Bouillard et al., 2014) applied on the *flexor digitimi minimi* muscle.

2. Acousto-elasticity in fibre muscle

2.1. Uniaxial stress in incompressible transversely isotropic solids

We model muscles as soft incompressible materials with one preferred direction, associated with a family of parallel fibres.

TI *compressible* solids are described by five independent constants, for example the following set (Rouze et al., 2020): $\mu_{\mathrm{L}}, E_{\mathrm{L}}, E_{\mathrm{T}}, \nu_{\mathrm{TT}}, \nu_{\mathrm{LT}}$, where μ_{L} is the shear elastic modulus relative to deformations along the fibres, E_{L}, E_{T} are the Young moduli along, and transverse to, the fibres, respectively, and ν_{TT}, ν_{LT} are the Poisson ratios in these directions. The shear elastic modulus μ_{T} relative to the transverse direction is $\mu_{\mathrm{T}} = \frac{E_{\mathrm{T}}}{2(1+\nu_{\mathrm{TT}})}$.

For *incompressible* TI materials, there is no volume change. This constraint leads to the following relations (see Rouze et al. (2020) for details),

$$\nu_{\mathrm{LT}} = \tfrac{1}{2}, \qquad \nu_{\mathrm{TT}} = 1 - \tfrac{E_{\mathrm{T}}}{2E_{\mathrm{L}}}. \tag{1}$$

Thus, only three independent constants are required to fully describe a given transversely isotropic, linearly elastic, incompressible solid. Here we choose the three material parameters $\mu_{\rm T}$, $\mu_{\rm L}$, and $E_{\rm L}$, as proposed by Li et al. (2016). Note that other, equivalent choices can be made (Chadwick, 1993; Rouze et al., 2013; Papazoglou et al., 2006).

We call x_1 the axis along the fibres and σ_{11} the uniaxial stress applied by the volunteers in that direction during the voluntary contractions. The resulting extension in that direction is e ($e > 0$: elongation, $e < 0$: contraction). Then a simple analysis (Chadwick, 1993) shows that $\sigma_{11} = E_{\rm L} e$, as expected.

2.2. Third-order expansion of the strain energy in a TI incompressible solid

Acousto-elasticity calls for a third-order expansion of the elastic strain energy W in the powers of $\boldsymbol{E}$, the Green-Lagrange strain tensor. For transversely isotropic incompressible solids, the expansion can be written as (Destrade et al., 2010a),

$$W = \mu_{\rm T} I_2 + \alpha_1 I_4^2 + \alpha_2 I_5 + \frac{A}{3} I_3 + \alpha_3 I_2 I_4 + \alpha_4 I_4^3 + \alpha_5 I_4 I_5, \tag{2}$$

where the second-order elastic constants α_1, α_2 are given by

$$\alpha_1 = \tfrac{1}{2}\left(E_{\rm L} + \mu_{\rm T} - 4\mu_{\rm L}\right), \qquad \alpha_2 = 2\left(\mu_{\rm L} - \mu_{\rm T}\right), \tag{3}$$

and A, α_3, α_4 and α_5 are third-order elastic constants. The strain invariants used in (2) are

$$I_2 = {\rm tr}(\boldsymbol{E}^2), \quad I_3 = {\rm tr}(\boldsymbol{E}^3), \quad I_4 = \boldsymbol{A}\cdot\boldsymbol{E}\boldsymbol{A}, \quad I_5 = \boldsymbol{A}\cdot\boldsymbol{E}^2\boldsymbol{A}, \tag{4}$$

where $\boldsymbol{A}$ is the unit vector in the fibres direction when the solid is unloaded and at rest. Note that Li and Cao (2020) call α_1 the $C_{\rm qSV}$ parameter, because it quantifies the spatial dependence of the speed $v_{\rm qSV}$ for the quasi shear vertical mode wave in an undeformed TI solid. Li and Cao (2020) show that α_1 can be negative or positive (with $2\alpha_1 > -4\mu_{\rm L}$, because $E_{\rm L} + \mu_{\rm T} > 0$).

For isotropic third-order elasticity, Gennisson et al. (2007) measured the parameter A for soft phantom gels and found that it can be positive or negative even for solids which have a similar second-order shear modulus μ. Hence they found $\mu = 8.5$ kPa, $A = -21.5$ kPa for a Gelatin-Agar phantom gel, and $\mu = 8.1$ kPa, $A = +10.7$ kPa for a PVA phantom gel. Thus there is a important difference from the nonlinear point of view between these two kinds of material even if their linear shear modulus are quite similar. As we will see, this remark carries over to TI muscle, where the hardening effect with effort proves to be much more important than the stiffness at rest.

2.3. Elastic waves in incompressible TI solids under uni-axial stress

We now study the propagation of small-amplitude plane body waves in a deformed, TI incompressible soft tissue. Destrade et al. (2010a) or Ogden and Singh (2011) show that it is equivalent to solving a 2×2 eigenproblem for the acoustical (symmetric) tensor. Its eigenvectors are orthogonal and give the two possible directions of transverse polarization; its eigenvalues are real and give the corresponding wave speeds.

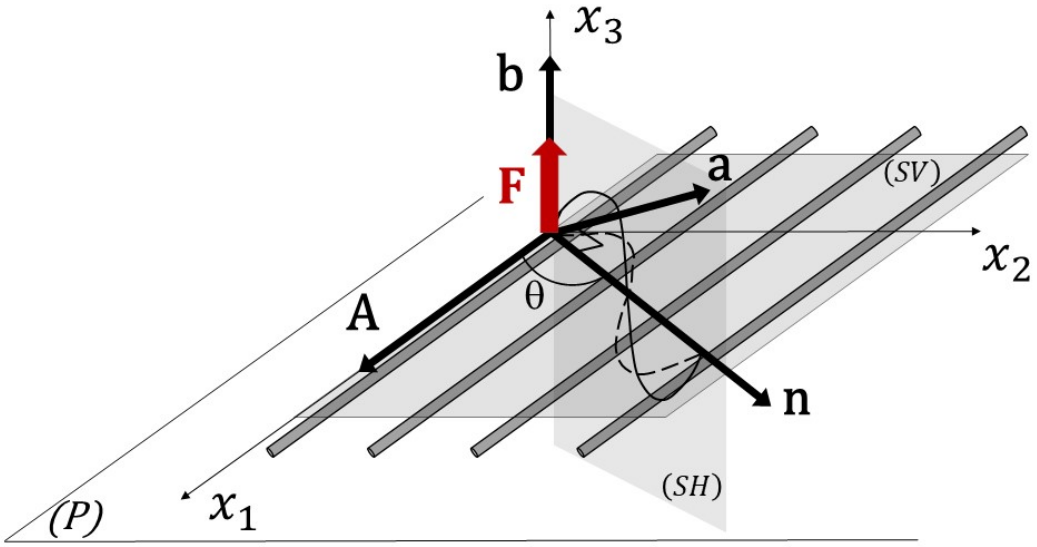

Figure 1: (P) is the $(\boldsymbol{A}, \boldsymbol{n})$-plane where $\boldsymbol{A}$ is a unit vector in the fibers direction when the solid is unloaded and at rest. $\boldsymbol{n}$ is a unit vector in the wave number direction. Two purely transverse waves propagates in a incompressible transversely isotropic solids: the polarized (SV) mode with the polarization $\boldsymbol{a}$ lies in the $(\boldsymbol{A}, \boldsymbol{n})$-plane; the polarized (SH) mode with the polarization $\boldsymbol{b}$ lies in the $(\boldsymbol{A} \times \boldsymbol{n}, \boldsymbol{n})$ plan. θ is the angle between $\boldsymbol{n}$ and $\boldsymbol{A}$. In our experiments, the radiation force $\boldsymbol{F}$ is along the x_3 axis. Ultrasound tracking measures the x_3 component of the shear wave displacement and is sensitive only to the (SH) propagation mode.

One eigenvector is $\boldsymbol{b} = \boldsymbol{A} \times \boldsymbol{n}$, orthogonal to both the fibres and the direction of propagation $\boldsymbol{n}$ (see Figure 1). It corresponds to the shear-horizontal (SH) wave mode. The second one is $\boldsymbol{a} = \boldsymbol{b} \times \boldsymbol{n}$ which lies in the (SV) plan. Calculations of these two wave speeds v evolution as a function of the uniaxial stress σ_{11} and the second and third order elastic moduli are given in Supplementary file (SP1). In our experiments, the radiation force $\boldsymbol{F}$ used to induce the transient shear wave is applied along the x_3 axis. Ultrasound tracking measures the x_3 component of the shear wave displacement and is sensitive only to the (SH) propagation mode. The (SH) mode speed v is given by

$$\rho v^2 = \mu_{\mathrm{L}} - \left[1 + \frac{1}{E_{\mathrm{L}}}\left(\mu_{\mathrm{L}} - \mu_{\mathrm{T}} + \frac{A}{4} + \alpha_3 + \frac{\alpha_5}{2}\right)\right]\sigma_{11} \tag{5}$$

for propagation *along the fibres*, and

$$\rho v^2 = \mu_{\mathrm{T}} + \frac{1}{E_{\mathrm{L}}}\left(3\mu_{\mathrm{T}} + \frac{A}{2} - \alpha_3\right)\sigma_{11} \tag{6}$$

for propagation *transversely to the fibres*. One can note that these equations correspond to equations (3) and (9) propose with a different approach in Bied et al. (2020).

Here ρ is the mass density, which remains constant throughout the deformation because of incompressibility. In this paper, we take $\rho = 1000$ kg/m^3, because most human soft tissues are assumed to have the same density as water. Notice that neither speed depends on the third-order constant α_4, and that the speed of waves travelling transversely to the fibres does not depend on μ_{L} and α_5 either. However, the longitudinal Young modulus E_{L} does appear in that speed's expression, showing the interplay of axial and transverse linear parameters in the acousto-elastic effect.

3. Materials and methods

3.1. Study purpose

Our goal is to measure the changes in the muscle stiffness, as measured by ρv^2 for the (SH) waves, as a function of the stress σ_{11} produced by a striated muscle during isometric contraction.

For this purpose, we use the Shear Wave Elastography (SWE) method, as provided by the Supersonic Shear Imaging (SSI) technique included into the Aixplorer Imaging System (Supersonic Imagine, Aix en Provence, France, version V12.3). In principle, shear viscosity, which is frequency-dependent, is expected to modify the shear wave speed measured by the SWE technique. However, if the shear viscosity is small compared to the shear elastic modulus, the dispersion effect is limited and the muscle can be considered as a purely elastic medium. Moreover, as shown by Bercoff et al. (2004), the effect of soft tissue viscosity on the shear wave speed is small provided the attenuation length is much larger than the wavelength.

We call $\mu = \rho v^2$ the "apparent shear modulus". In our *in vivo* study, we measure the changes in $\mu_{\parallel} = \mu_{\parallel}(\sigma_{11})$ along the fibre direction and the changes in $\mu_{\perp} = \mu_{\perp}(\sigma_{11})$ transversely to the fibre direction, with the axial stress σ_{11} produced by the muscle. Then we use inverse analysis to link these experimental results to the acoustic-elasticity theory developed in Section 2. We carry an *in vivo* feasibility study on six healthy volunteers with different age and sex.

3.2. Muscle and imaging plane

The structure of muscles is complicated by inhomogeneities in fibre orientation and interfaces between fibre bundles. To isolate the behaviour of an individual muscle, unaffected by the complementary or antagonistic actions of other muscles, we select the *flexor digiti minimi* muscle, which extends the hand's little finger.

This muscle is the only one involved in the little finger's extension, it has homogeneous fibre orientation (TI symmetry), and it is close to the epidermis, which matters for the relatively high frequency probe (SLH20-6 SSI probe, 12 MHz center frequency) used for the SWE measurements. Furthermore, as shown in Figures 2-3, this

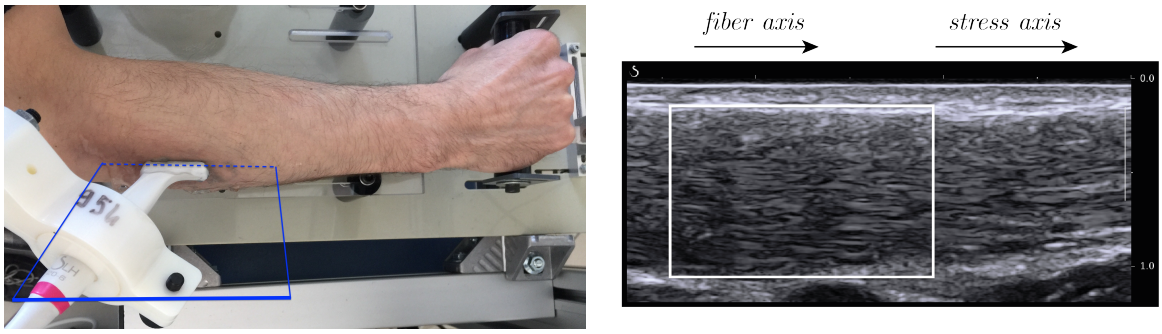

Figure 2: (a) SLH20-6 musculoskeletal probe placed above the right hand *flexor digiti minimi* muscle in the fibre direction. (b) Bmode image (26.7 × 14.7 mm) in the probe plane showing the fibres. The muscle studied is at a depth between 0.5 and 1 cm.

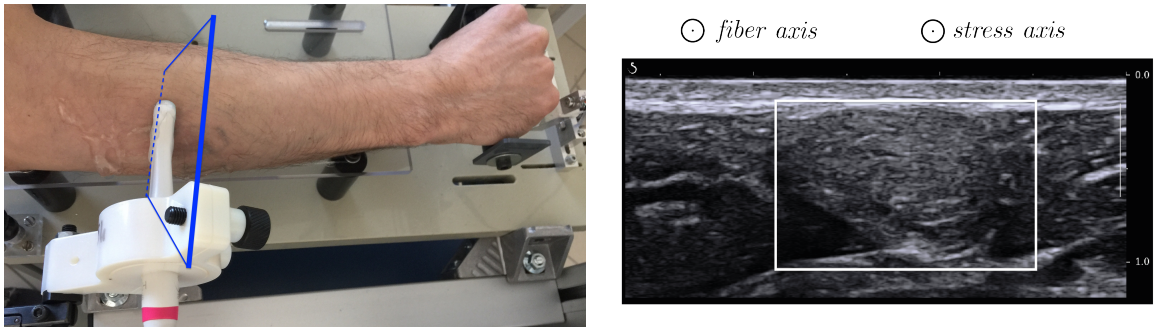

Figure 3: (a) Probe placed above the right hand *flexor digiti minimi* muscle perpendicularly to the fibre direction. (b) Corresponding Bmode image (26.7 × 14.7 mm), showing that the muscle is almost circular, see center of the image.

muscle is convenient for probing, as it is situated on the side at the top of the forearm and spans over a distance longer than the 26.7 mm imaging width of the SLH20-6 probe.

The quality of the ultrasound imaging system is important for the probe positioning and the localisation of the muscle, which has a diameter of about 0.6 cm. One way to precisely localize the muscle on the image is to move slowly the little finger and look at the lateral tissue displacement in real time, with the probe positioned in the fibre direction. As shown on Figures 2(a) and 3(a), the probe is held axially and transversely to the fibre direction by a free arm stand, which can be locked in the desired position. We took particular care not to apply pressure with the probe on the skin surface. Bmode images of the right hand *flexor digiti minimi* are shown on Figures 2(b) and 3(b), for a representative subject at rest. The image dimension is 14.7 mm depth by 26.7 mm width, giving an idea of the small size of the muscle. The white boxes delimit the region of interest, where SWE data are acquired.

(a) The subject is seated with their right elbow flexed at 135° (180° corresponds to the full extension of the elbow) and positioned vertically at approximately 70° to the body.

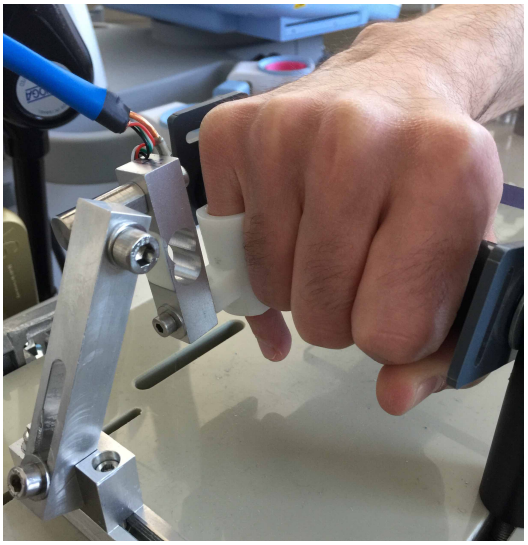

(b) The little finger's first phalanx is placed vertically and in contact with a cylindrical rigid interface. The finger is aligned with the force sensor.

Figure 4: Experimental setup including the custom-made force measurement system and the US Aixplorer imaging system running the SonicLab V12 research software to upload the Shear Wave Elastography (SWE) sequence.

3.3. Protocol and participants

Figure 4 shows the experimental setup including the custom-made force measurement system and the ultrasound imaging system.

Two women and four men, all right-handed, took part in this feasibility trial. They were informed of the possible risk and discomfort associated with the experimental procedures prior to giving their written consent to participate. Neither pregnant women nor persons under guardianship were included. The experimental design of this study was approved by the local Ethical Committee (Number ID RCB: 2020-A01601-38) and was carried out in accordance with the Declaration of Helsinki.

The subjects are seated with their right elbow flexed to 135° (180° corresponds to the full extension of the elbow) and positioned vertically at approximately 70° to the body. The first phalanx of the little finger is placed vertically and in contact with a cylindrical rigid interface (Figure 4b), so that it is aligned with the calibrated force sensor (micro load cell CZL635-20) and at rest.

First, we asked the subjects to perform three maximum isometric voluntary contractions (MVC) lasting at least 3 seconds and separated by 30 seconds of recovery. The largest of the three forces was considered as the maximum voluntary force and was used to normalize subsequent submaximal contractions.

Table 1 details the age, genre, handedness, maximum voluntary force developed with the little finger, diameter of the muscle and finally, the maximum axial stress $\sigma_{11\text{Max}}$

calculated by dividing the MVC force by the current muscle cross-surface area (obtained using the Bmode image in the direction transverse to the fibre direction). Interestingly, in spite of their great age difference (40 years), Subject#2 and Subject#3 (both male) develop the same maximum force magnitude (the maximum lifted load difference is only 26 g) but Subject#2 has twice the muscle cross-surface area as Subject#3. Thus the maximum voluntary stress $\sigma_{11\text{Max}}$ induced by Subject#2 is half that of Subject#3. On the other hand, the axial stress $\sigma_{11\text{Max}}$ obtained by Subject#5 is one of the smallest in the cohort, while its maximum lifted load is the largest. We also note that the maximum voluntary force range is large, from a low of 5.25 N for Subject#4 to a high of 9.06 N for Subject#5.

Table 1: Age, Gender, R/L Handedness, Maximum Lifted Load, Maximum Volontary Force, *flexor digiti minimi* muscle surface and maximum axial stress $\sigma_{11\text{Max}}$ for the six healthy volunteers involved in the feasibility trial.

Subject	Age (years)	Genre (M/F)	Handedness R/L	Maximum Load Lifted (g)	Maximum Volontary Force (N)	Muscle Surface (cm^2)	$\sigma_{11\text{Max}}$ (kPa)
#1	22	M	R	630	6.30	0.28	225
#2	62	M	R	725	7.25	0.27	268
#3	22	F	R	699	6.99	0.14	499
#4	25	F	R	525	5.25	0.2	262
#5	40	M	R	906	9.06	0.5	181
#6	32	M	R	902	9.02	0.55	164

Then the participants were asked to perform five voluntary contractions at levels corresponding to 4, 8, 12, 16, 20% of MVC. They had to stay 4 seconds at each stage before moving to the next level. This period provided sufficient time to save the SWE image on the Aixplorer (and to allow for some viscous dissipation). To control the force steps, the participants followed a visual feedback displayed on a monitor placed in front of them, see Figure 4a. It turned out to be difficult for some subjects to maintain precisely a constant force, especially at the 16% and 20% levels of the maximal voluntary contraction. For this reason we conducted our inverse analysis for measurements up to 12% only, see results in Section 4.

3.4. Shear Wave Elastography measurements

We used the Shear Wave Elastography method to measure how shear elasticity changed with the force applied by the volunteers during the isometric contraction protocol.

The SWE experiment is based on two steps: the generation of the shear waves and the ultrafast imaging of their propagation. In our experiments, the central frequency of the fast imaging scheme is 7.5 MHz and the image repetition frequency is set to 14 kHz, adapted to muscle stiffness.

There are 48 frames in the temporal dimension, with a spatial resolution of 71.4 μs. Hence, we record the SW propagation for 3.4 ms, which is sufficient to follow the wave propagating along the width of the probe. The time $t = 0$ ms in Figure 5 correspond to the beginning of the SWE data acquisition which is situated ()ms after the beginning of the push sequence. There are 44 sampling points along the vertical axis, between the depths of 2.3 mm and 11.2 mm, with an axial resolution corresponding to one ultrasonic wavelength at 7.5 MHz, i.e 205 μm. There are 110 sampling points along the x_1 axis, between $(x_1)_0 = 1.5$ mm and $(x_1)_{\text{Max}} = 16.8$ mm, with the lateral resolution of SLH20-6 probe pitch being 140 μm.

An SWE acquisition consists of five pushing lines positioned at -0.23, 3.77, 7.77, 11.77, 15.77 mm, with two focal points at 6.7 mm and 9.7 mm.

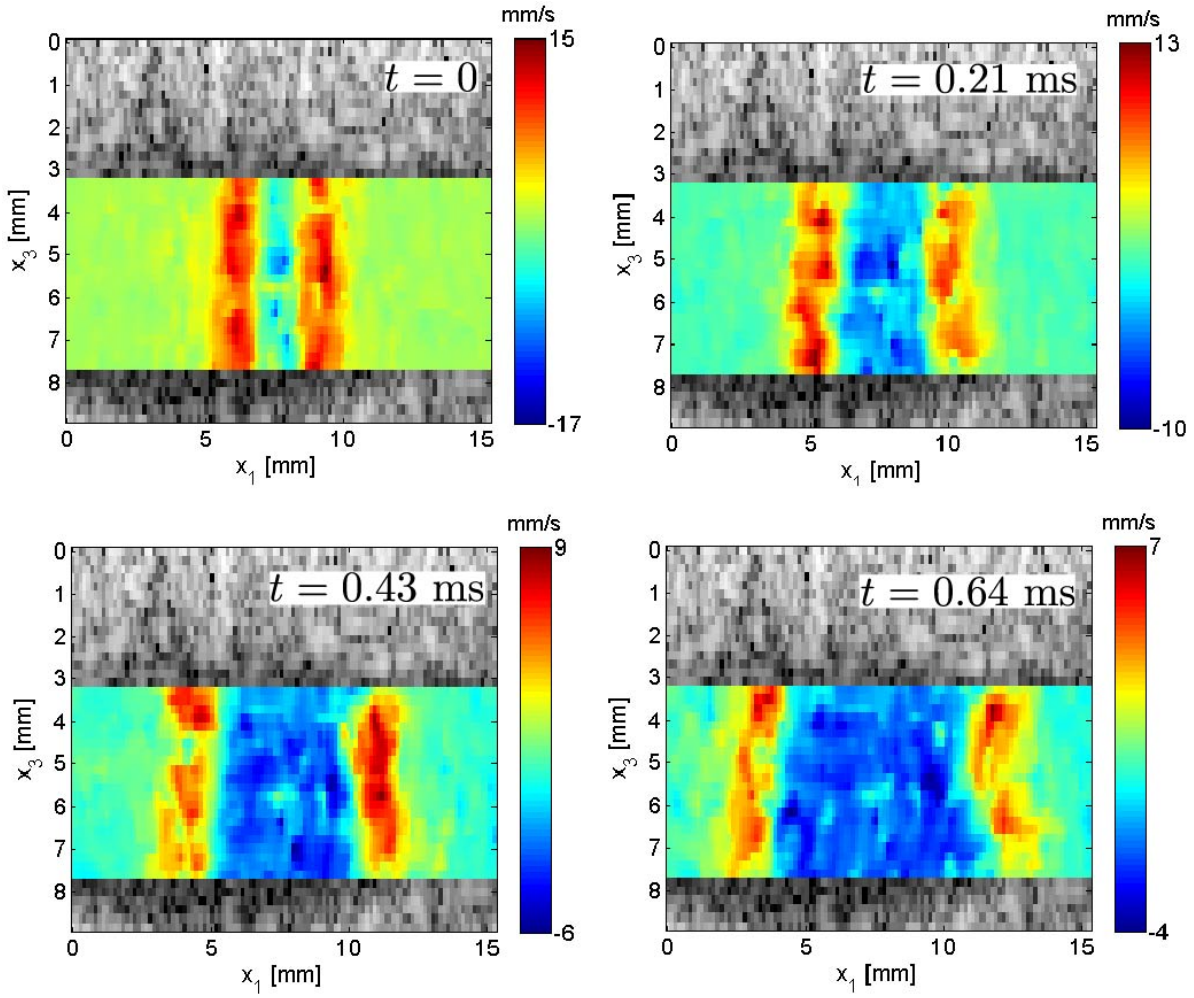

Figure 5: Shear wave (SH mode) propagation along the *flexor digiti minimi* muscle fibres for Subject#5 at rest. The wave propagates in the fibres direction x_1 and is polarized vertically along the x_3 axis. The color gives the tissue particle velocity at each location, see scale on the right (which adapts for better visualization).

4. Results

4.1. Propagation along the fibres

Figure 5 shows the shear wave propagation induced in the muscle by the ultrasonic transient radiation force for Subject#5 at rest. The radiation force is applied vertically along the positive x_3 axis. The wave propagates in the fibre direction along the x_1 axis and is polarized along the x_3 axis. The propagation is presented at four different times: $t = 0, 0.21, 0.43, 0.64$ ms, with a color scheme for the speed value, superimposed onto the Bmode image. The color scale is adapted for each image to take into account wave attenuation and enhance visualization. Note that here the Bmode image is obtained from the shear wave tracking sequence and has a lower quality than the Bmode image shown in Figure 2. For this figure, we selected the third push zone situated at the lateral position 7.77 mm.

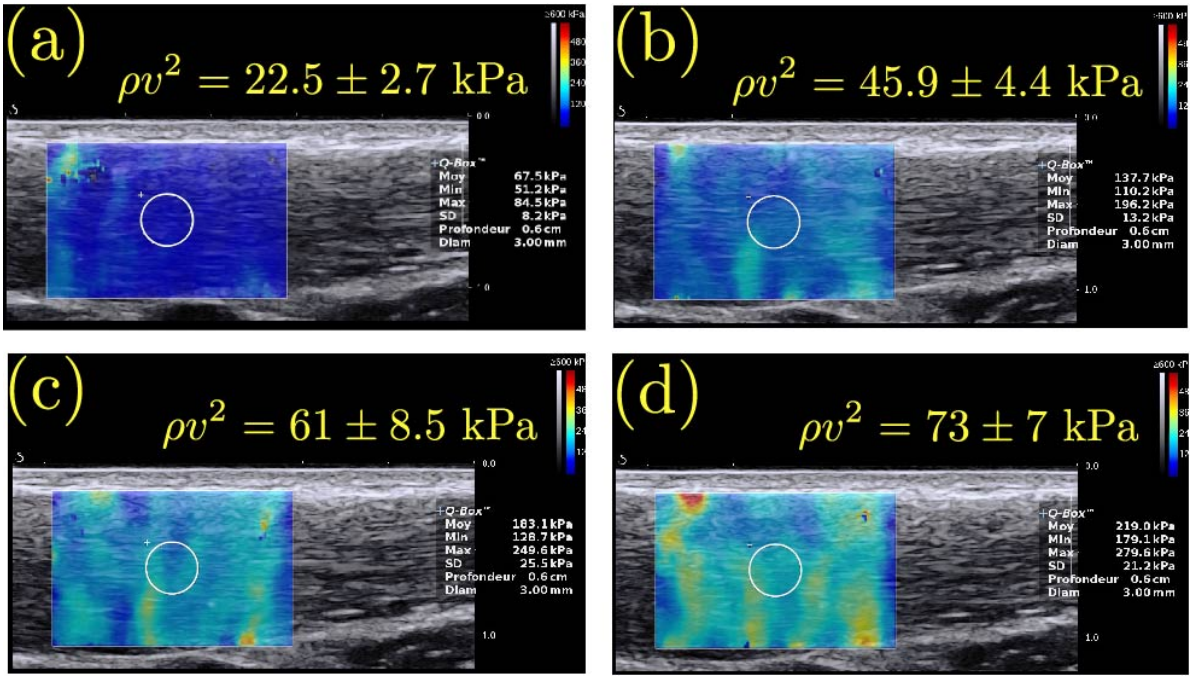

Figure 6: SWE analysis for Subject#5 at four levels of voluntary contraction along the *flexor digiti minimi* muscle fibres. (a): at rest, (b): 4% MVC, (c): 8% MVC, (d): 12% MVC. From the Aixplorer measure we deduce the average wave speed in the ROI (disc inside white circle) and compute the apparent axial shear modulus $\mu_{\parallel}(\sigma_{11}) = \rho v^2$. For this subject, it increases with the applied stress.

At time $t = 0.64$ ms, we can clearly see that the lower part of the shear wave front is ahead of the other parts of the wave front, indicating that the wave propagates faster in the muscle. Thus, we select the region of interest (ROI) in that part of the picture, from $x_3 = 6.2$ to $x_3 = 7.7$ mm (6 points), where the speed v is assumed homogeneous to average the lateral propagation and improve the signal-to-noise ratio.

We assume that the phase speed dispersion is small at that the SWE measurement gives the speed of all shear waves with different frequencies in the wave packet. Further, we assume that viscosity might attenuate the amplitude of the wave, but does not modify its speed noticeably (Bercoff et al., 2004).

Figures 6 show the measurements given by the SWE diagnostic mode of the Aixplorer, obtained for Subject#5 at four levels of voluntary contraction: 0, 4, 8, 12 % of MVC, corresponding to σ_{11} equal to 0, 7.2, 14.5, and 21.7 kPa, respectively. The machine gives a "stiffness" value, obtained by multiplying ρv^2 by 3 to yield the apparent isotropic Young modulus. However here the material is anisotropic and we cannot use that formula. Instead we simply divide back the machine mean value over the selected ROI (say 67.5 ± 8.2 kPa at rest, Figure 6(a)) by 3 (to obtain $\rho v^2 = 22.5 \pm 2.7$ kPa at rest, for example).

We collected the measurements on Figure 7(a) for the six volunteers. We notice a linear variation of $\mu_{\parallel}(\sigma_{11})$ with σ_{11} in the fibres direction, similar to the behaviour obtained experimentally by Bouillard et al. (2011) on the *abductor digitimi minimi* muscle. This variation is also in line with our theoretical analysis, according to which $\mu_{\parallel}(\sigma_{11}) = \rho v^2$ is given by (5), as

$$\mu_{\parallel}(\sigma_{11}) = \mu_{\mathrm{L}} - \beta_{\parallel}\sigma_{11}, \tag{7}$$

where the (non-dimensional) coefficient of nonlinearity $\beta_{\parallel}$ is defined as

$$\beta_{\parallel} = 1 + \frac{1}{E_{\mathrm{L}}}\left(\mu_{\mathrm{L}} - \mu_{\mathrm{T}} + \frac{A}{4} + \alpha_3 + \frac{\alpha_5}{2}\right), \tag{8}$$

For all six subjects, $\mu_{\parallel}(\sigma_{11})$ increases with σ_{11}, so that $\beta_{\parallel} < 0$ in the cohort.

For the curve-fitting exercise determining the quantities μ_{L} and $\beta_{\parallel}$, we use the Matlab *robustfit* algorithm which allocates lower weight to points that do not fit well. It also outputs the coefficient of determination R^2 and the root mean squared error $\mathrm{RMS_e}$.

4.2. Propagation across the fibres

In the direction transverse to the muscle fibres, the shear wave is highly scattered by heterogeneities, which induces a poor signal-to-noise ratio for frequency analysis (Deffieux et al., 2008b).

Figures 8 show the shear wave propagation perpendicularly to the fibres axis for Subject #5, at four different times: $t = 0, 0.29, 0.58, 0.87$ ms. Superimposed onto the Bmode image, we show the propagation inside the muscle only, which has a quasi-circular shape with a diameter of approximately 8 mm (see Figure 3 for a more precise localisation of the muscle with a better Bmode image quality).

Figures 9 show the values of the apparent shear modulus $\mu_{\perp}(\sigma_{11}) = \rho v^2$ in the transverse direction, for Subject#5. Again, we present measurements up to 12% of MVC.

According to our theoretical analysis, $\mu_{\perp}(\sigma_{11})$ is equal to ρv^2 given by (6) as

$$\rho v_{\mathrm{b}}^2 = \mu_{\perp}(\sigma_{11}) = \mu_{\mathrm{T}} - \beta_{\perp}\sigma_{11}, \tag{9}$$

where

$$\beta_{\perp} = \frac{1}{E_{\mathrm{L}}}\left(3\mu_{\mathrm{T}} + \frac{A}{2} - \alpha_3\right). \tag{10}$$

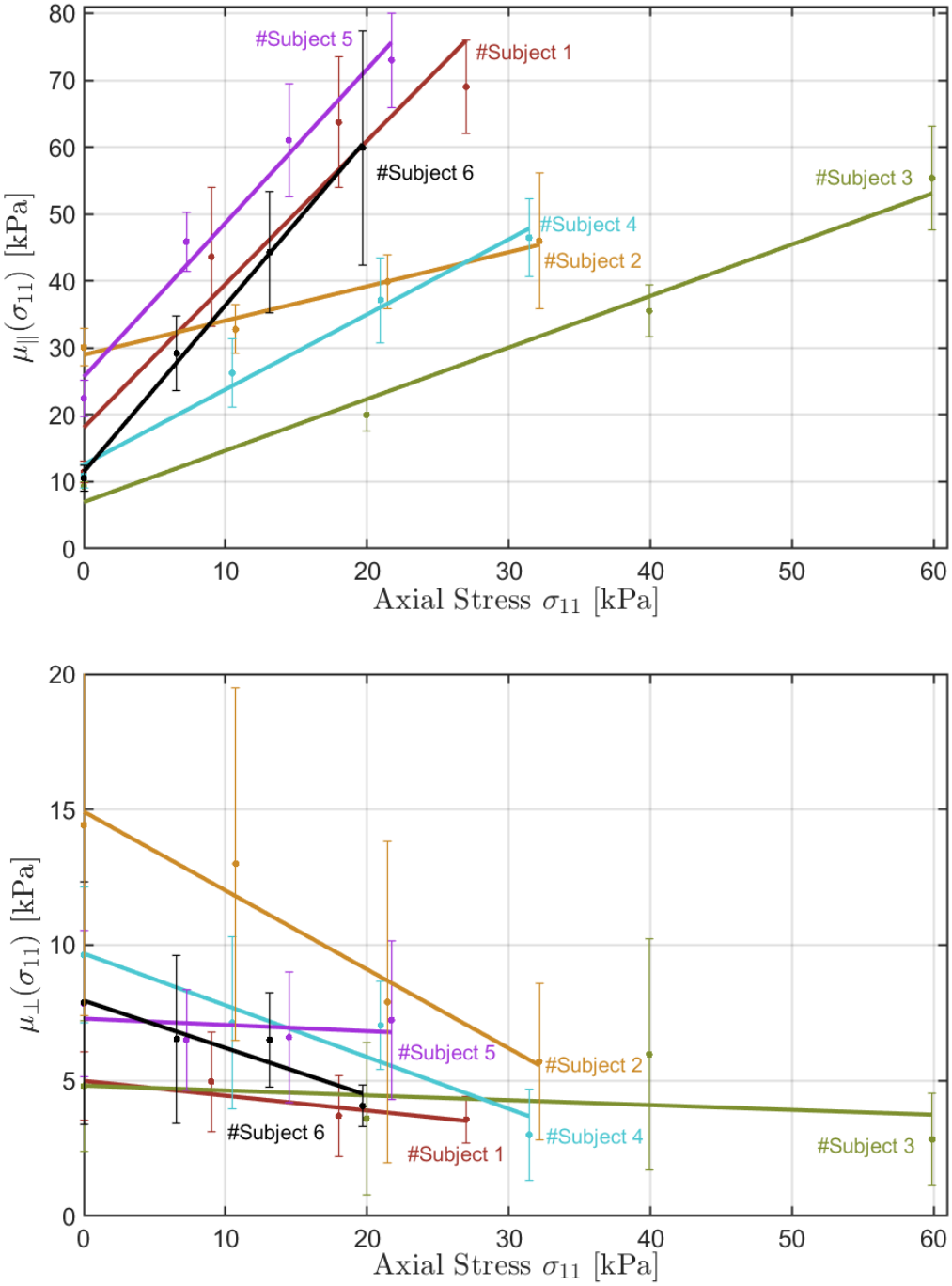

Figure 7: Apparent shear elastic modulus $\rho v^2\,(\sigma_{11})$ changes with the axial stress σ_{11}, measured *in vivo* by SWE on the *flexor digiti minimi* muscle (a) along the fibres axis $\mu_{\parallel}\,(\sigma_{11})$ and (b) across the fibres axis $\mu_{\perp}\,(\sigma_{11})$ for the six subjects of our feasibility study.

Again, we use the formula from acoustic-elasticity theory to produce a linear fit to the data. In contrast to the case of propagation along the fibres, we find that $\mu_\perp(\sigma_{11})$ does not increase with the axial stress σ_{11}, but decreases slightly for Subject#5. Other subjects lead to different behaviours, as can be checked on Figure 7(b).

We summarise the results in Table 2.

5. Discussion

Using acousto-elasticity theory, we obtained analytical expressions for the dependence of the SH shear wave speed as a function of the applied uniaxial stress in muscle, assuming that it behaves as a transversely isotropic, incompressible soft solid, and that the wave travels either along or transverse to the fibres.

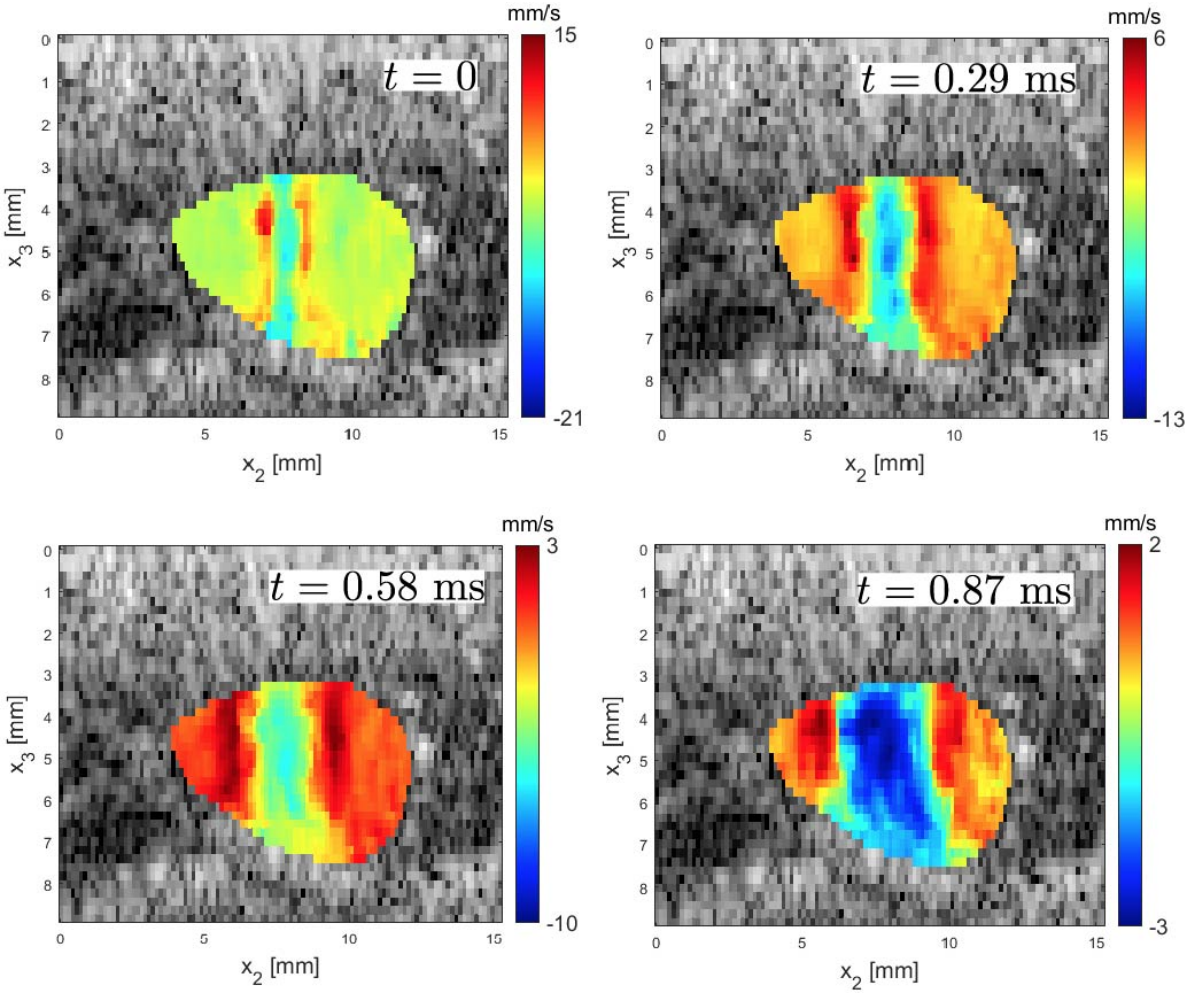

Figure 8: Shear wave (SH mode) propagation transversely to the *flexor digiti minimi* muscle fibres for Subject#5 at rest. The wave propagates along the x_2 axis and is polarized vertically along the x_3 axis. The color gives the tissue particle velocity at each location, see scale on the right (which adapts for better visualization)

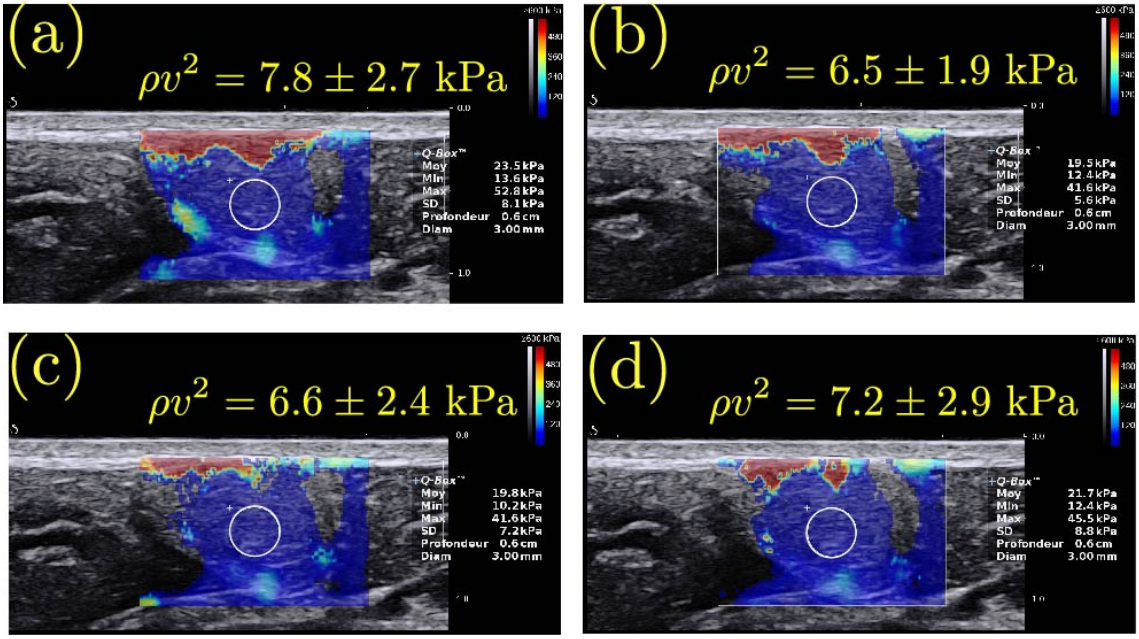

Figure 9: SWE analysis for Subject#5 at four levels of voluntary contraction transversely to the *flexor digiti minimi* muscle fibres. (a): at rest, (b): 4% MVC, (c): 8% MVC, (d): 12% MVC. From the Aixplorer measure we deduce the average wave speed in the ROI (disc inside white circle) and compute the apparent transverse shear modulus $\mu_\perp(\sigma_{11}) = \rho v^2$. For this subject, the apparent modulus decreases slightly with the applied stress.

Table 2: Axial shear elastic modulus at rest μ_{L}, axial nonlinearity coefficient $\beta_{\parallel}$, transverse shear elastic modulus at rest μ_{T}, transverse nonlinearity parameter $\beta_\perp$, 12% of maximum axial stress $\sigma_{11\mathrm{Max}}$ for the *flexor digiti minimi* muscle of the six healthy volunteers involved in the study.

Subject	μ_{L} (kPa)	$\beta_{\parallel}$	R^2	μ_{T} (kPa)	$\beta_\perp$	R^2	$0.12\sigma_{11\mathrm{Max}}$ (kPa)
#1	18.1 ± 8.9	-2.14 ± 0.53	0.89	5.0 ± 0.4	0.05 ± 0.02	0.72	27.0
#2	29.0 ± 1.3	-0.51 ± 0.07	0.97	14.9 ± 1.0	0.29 ± 0.05	0.94	32.2
#3	6.9 ± 3.0	-0.77 ± 0.08	0.98	4.8 ± 1.5	0.02 ± 0.04	0.09	59.9
#4	12.6 ± 2.1	-1.12 ± 0.10	0.98	9.7 ± 1.0	0.19 ± 0.05	0.87	31.4
#5	25.7 ± 3.9	-2.30 ± 0.30	0.96	7.3 ± 0.7	0.02 ± 0.05	0.09	21.7
#6	11.5 ± 1.2	-2.50 ± 0.09	0.99	7.9 ± 0.6	0.17 ± 0.05	0.85	19.7

For our experiments, we oriented the acoustic radiation force along the vertical axis and propagated the wave along or transverse to the *flexor digiti minimi* muscle to avoid coupling of the shear horizontal (SH) mode with the shear vertical (SV) mode (Rouze et al., 2020). We determined theoretically and experimentally the apparent shear elastic modulus $\mu\left(\sigma_{11}\right) = \rho v^2$, and found it varies linearly with σ_{11}.

We obtained analytical expressions for $\mu_{\parallel}\left(\sigma_{11}\right) = \mu_{\mathrm{L}} - \beta_{\parallel}\sigma_{11}$ in the fibre direction

and for $\mu_\perp(\sigma_{11}) = \mu_T - \beta_\perp \sigma_{11}$ transversely to the fibre direction. The coefficient $\beta_\parallel$ is a linear combination of the second-order elastic parameters μ_L, μ_T, E_L, and the third-order moduli A, α_3, α_5; the coefficient $\beta_\perp$ is written in terms of only two second-order parameters μ_T, E_L and two third-order moduli A, α_3. Neither coefficient involves the other third-order parameter α_4.

Our *in vivo* analysis of the six-volunteer cohort focused on the variation of the apparent shear elastic moduli with σ_{11}. The results show that these variations are very different across the cohort.

For the analysis of $\mu_\perp(\sigma_{11})$, we distinguish three subgroups.

For Subjects #2,4,6 (first group), we find $\beta_\perp = 0.29, 0.19, 0.17$ (± 0.05) , respectively, all positive, indicating that $\mu_\perp$ decreases with σ_{11}. Here the connective tissue surrounding the muscle fibres softened under axial stress σ_{11}.

For Subjects #1,3,5, we find $\beta_\perp = 0.05 \pm 0.02, 0.02 \pm 0.04, 0.02 \pm 0.05$, respectively, all small values, indicating that $\mu_\perp$ is almost unchanged as σ_{11} increases. For these three subjects, the infinitesimal shear elastic moduli μ_T are almost the same: $\mu_T = 5.0 \pm 0.4, 4.8 \pm 1.5, 7.3 \pm 0.7$ kPa, respectively. However, Subject#3 has a much greater value of 12% of maximum axial stress ($12\%\sigma_{11\text{Max}} = 59.9$ kPa) than Subjects#1,5, who have approximately the same value (27.0, 21.7 kPa, respectively). Subject#3 also has a much lower magnitude of coefficient $\beta_\parallel$ $(= -0.77 \pm 0.08)$ than Subjects#1,5 who have approximately the same $\beta_\parallel$ coefficient $(= -2.14 \pm 0.53, -2.3 \pm 0.30)$. Thus, we separate Subjects#1,5 (second group) from Subject#3 (third group).

By comparing expressions (8) and (10) for the β nonlinearity coefficients, we see that only the μ_L and α_5 parameters can explain why $\beta_\parallel$ is different between the second and the third group, because they do not appear in the expression (10) for $\beta_\perp$ (which is the same for these two groups). Hence we see that a higher value of μ_L in (8) results in a higher value of the coefficient $\beta_\parallel$ for subjects who have an identical $\beta_\perp$. This is indeed what we observed experimentally, see values in Table 2.

Finally, we note that both the combination of linear moduli $\mu_L - \mu_T$ and the nonlinearity coefficient $\beta_\perp$ are positive for all Subjects.

For the analysis of the axial apparent shear modulus $\mu_\parallel(\sigma_{11})$, we also find three subgroups, according to the magnitude of the nonlinearity coefficient $\beta_\parallel$. Hence Subjects#2,3 both present small magnitudes for $\beta_\parallel$, Subject#4 present intermediate value, and Subjects#1,5,6 all present high values (in that order).

For a contraction from rest to 12% MVC, Subject#6's apparent elastic modulus $\mu_\parallel(\sigma_{11})$ increases by a factor 6, from 10.5 to 59.9 kPa, demonstrating his remarkable ability to recruit fibres to harden the muscle very quickly. On the *peroneus longus* muscle of anaesthetised cats, Petit et al. (1990) found that the S motor units can produce high values of muscle stiffness, suggesting that for Subject#6, the motor units ratio S/F might be very high. Subject#6 also develops the smallest 12% of maximum axial stress value of the cohort, consistent with a high S/F ratio because slow (S) motor units develop quite small tensions compared with fast fatigue-resistant (FR) and fast fatiguable (FF) units Petit et al. (1990).

For Subjects#1,5,6 (third group), we note that the increase in the magnitude of $\beta_{\|}$ is associated with a decrease of the maximal axial stress $\sigma_{11\mathrm{Max}}$.

For Subjects#2,3 (first group), we recorded the smallest magnitude of the nonlinearity coefficient $\beta_{\|}$ ($-0.51 \pm 0.07, -0.77 \pm 0.08$, respectively). These two subjects develop respectively the second-highest (32.2 kPa) and the highest (59.9 kPa) maximum axial stress $12\%\sigma_{11\mathrm{Max}}$ in the cohort. These results are consistent with a high presence of fast fibres (F) that do not harden rapidly the muscle, associated with a quite high tension Petit et al. (1990).

A natural follow-up on this study is to apply the method to patients with musculoskeletal disorders or neurodegenerative diseases. However, the method must be adapted because we found it was difficult for some healthy subjects to maintain a voluntary constant force during the time required to measure the wave speed, a task which could prove even more challenging for patients. This adaptation could be achieved with a muscle contained hardening method, based on the corresponding nerve electro-stimulation associated with a synchronous measurement of force and elasticity. That set up would provide a calibrated and repeatable stimulation protocol as used for EMG measurements. A better localisation of the muscle and a better probe positioning in relation to the fibres orientation could be achieved by linking in real time the ultrasound Bmode image with the corresponding slice plan of a pre-acquired MRI volume image. Finally, the modelling could be improved, to include heterogeneity, viscosity and dispersion.

6. Conclusion

The quantification of the elastic nonlinearity of biological tissues can prove to be a most valuable tool for the early diagnosis of musculoskeletal disorders. Here, we developed an acousto-elasticity theory to study the propagation of small-amplitude plane body waves in deformed transversely isotropic incompressible solids. For the shear horizontal (SH) mode, we obtained a linear relation between the wave speed ρv^2 and the applied axial stress σ_{11} using the second- and third-order elastic constants. Then we used this theory to analyse experimental results on skeletal striated muscle.

With a cohort of six healthy volunteers, we uncovered a great diversity for the nonlinear behaviour of the *flexor digiti minimi* muscle, for the apparent shear modulus $\mu_{\|}(\sigma_{11})$ along the fibres as well as for the transverse apparent shear modulus $\mu_{\perp}(\sigma_{11})$. Hence $\mu_{\perp}$ can decrease with σ_{11} (Subjects#2,4,8), increase (Subjects#5,6) or remain almost constant (Subjects#1,3,7). Meanwhile, $\mu_{\|}$ always increases with σ_{11}, and the rate of increase is highly correlated to the weakness of the maximum voluntary contraction produced by the volunteer.

Acknowledgments

We thank Véronique Marchand-Pauvert (Laboratoire d'Imagerie Biomédicale, Sorbonne

Université) for helpful discussions about the role of motor units in muscle function and their relationship to muscle elasticity. We also thank Jean-Marc Gregoire and Jean-Yves Tartu (iBrain Laboratory, Université de Tours) for the development of the electronics and the mechanics of the force measurement device, respectively. This work is supported by the Institut du Biomédicament and by the INCA Plan Cancer BPALP project.

References

P. F. Adams and M. A. Marano. Current estimates from the national health interview survey. *Vital and Health Statistics. Series 10, Data from the National Health Survey*, (193 Pt 1):1, 1995.

E. M. Badley, I. Rasooly, and G. K. Webster. Relative importance of musculoskeletal disorders as a cause of chronic health problems, disability, and health care utilization: findings from the 1990 Ontario Health Survey. *The Journal of Rheumatology*, 21(3): 505–514, 1994.

M. Bayat, S. Adabi, V. Kumar, A. Gregory, J. Webb, M. Denis, B. Kim, A. Singh, L. Mynderse, and D. Husmann. Acoustoelasticity analysis of transient waves for non-invasive in vivo assessment of urinary bladder. *Scientific Reports*, 9(1):1–9, 2019.

J. Bercoff, M. Tanter, M. Muller, and M. Fink. The role of viscosity in the impulse diffraction field of elastic waves induced by the acoustic radiation force. *IEEE transactions on Ultrasonics, Ferroelectrics, and Frequency Control*, 51(11):1523–1536, 2004.

M. Bernal, F. Chamming's, M. Couade, J. Bercoff, M. Tanter, and J.-L. Gennisson. In vivo quantification of the nonlinear shear modulus in breast lesions: Feasibility study. *IEEE Transactions on Ultrasonics, Ferroelectrics, and Frequency Control*, 63 (1):101–109, 2015.

M. Bied, L. Jourdain, and J.-L. Gennisson. Acoustoelasticity in transverse isotropic soft tissues: quantification of muscles' nonlinear elasticity. In *2020 IEEE International Ultrasonics Symposium (IUS)*, pages 1–4. IEEE, 2020.

K. Bouillard, A. Nordez, and F. Hug. Estimation of individual muscle force using elastography. *PloS One*, 6(12), 2011.

K. Bouillard, M. Jubeau, A. Nordez, and F. Hug. Effect of vastus lateralis fatigue on load sharing between quadriceps femoris muscles during isometric knee extensions. *Journal of Neurophysiology*, 111(4):768–776, 2014.

P. Chadwick. Wave propagation in incompressible transversely isotropic elastic media I. Homogeneous plane waves. *Proceedings of the Royal Irish Academy.*, pages 231–253, 1993.

T. Deffieux, J.-L. Gennisson, M. Tanter, and M. Fink. Assessment of the mechanical properties of the musculoskeletal system using 2-D and 3-D very high frame rate ultrasound. *IEEE Transactions on Ultrasonics, Ferroelectrics, and Frequency Control*, 55(10):2177–2190, 2008a.

T. Deffieux, G. Montaldo, M. Tanter, and M. Fink. Shear wave spectroscopy for in vivo quantification of human soft tissues visco-elasticity. *IEEE Transactions on Medical Imaging*, 28(3):313–322, 2008b.

M. Destrade, M. D. Gilchrist, and R. W. Ogden. Third-and fourth-order elasticities of biological soft tissues. *The Journal of the Acoustical Society of America*, 127(4): 2103–2106, 2010a.

M. Destrade, M. D. Gilchrist, and G. Saccomandi. Third-and fourth-order constants of incompressible soft solids and the acousto-elastic effect. *The Journal of the Acoustical Society of America*, 127(5):2759–2763, 2010b.

J. D'hooge, A. Heimdal, F. Jamal, T. Kukulski, B. Bijnens, F. Rademakers, L. Hatle, P. Suetens, and G. R. Sutherland. Regional strain and strain rate measurements by cardiac ultrasound: Principles, implementation and limitations. *European Journal of Echocardiography*, 1(3):154–170, 2000.

M. E. Downs, S. A. Lee, G. Yang, S. Kim, Q. Wang, and E. E. Konofagou. Non-invasive peripheral nerve stimulation via focused ultrasound in vivo. *Physics in Medicine & Biology*, 63(3):035011, 2018.

A. Eranki, N. Cortes, Z. G. Ferenček, and S. Sikdar. A novel application of musculoskeletal ultrasound imaging. *Journal of Visualized Experiments)*, (79):e50595, 2013.

L. Ford, A. Huxley, and R. Simmons. The relation between stiffness and filament overlap in stimulated frog muscle fibres. *The Journal of Physiology*, 311(1):219–249, 1981.

J.-L. Gennisson, S. Catheline, S. Chaffai, and M. Fink. Transient elastography in anisotropic medium: Application to the measurement of slow and fast shear wave speeds in muscles. *The Journal of the Acoustical Society of America*, 114(1):536–541, 2003.

J.-L. Gennisson, M. Rénier, S. Catheline, C. Barrière, J. Bercoff, M. Tanter, and M. Fink. Acoustoelasticity in soft solids: Assessment of the nonlinear shear modulus with the acoustic radiation force. *The Journal of the Acoustical Society of America*, 122(6):3211–3219, 2007.

J.-L. Gennisson, T. Deffieux, E. Macé, G. Montaldo, M. Fink, and M. Tanter. Viscoelastic and anisotropic mechanical properties of in vivo muscle tissue assessed by supersonic shear imaging. *Ultrasound in Medicine & Biology*, 36(5):789–801, 2010.

K. Gijsbertse, R. Goselink, S. Lassche, M. Nillesen, A. Sprengers, N. Verdonschot, N. van Alfen, and C. De Korte. Ultrasound imaging of muscle contraction of the tibialis anterior in patients with facioscapulohumeral dystrophy. *Ultrasound in Medicine & Biology*, 43(11):2537–2545, 2017.

F. Hug, K. Tucker, J.-L. Gennisson, M. Tanter, and A. Nordez. Elastography for muscle biomechanics: Toward the estimation of individual muscle force. *Exercise and Sport Sciences Reviews*, 43(3):125–133, 2015.

L. Jacobson, B. Lindgren, and V. Sjukdomarna. What are the costs of illness? *Stockholm: Socialstyrelsen (National Board of Health and Welfare)*, 1996.

Y. Jiang, G. Li, L.-X. Qian, S. Liang, M. Destrade, and Y. Cao. Measuring the linear and nonlinear elastic properties of brain tissue with shear waves and inverse analysis. *Biomechanics and Modeling in Mechanobiology*, 14(5):1119–1128, 2015.

K. Kim, H.-J. Hwang, S.-G. Kim, J.-H. Lee, and W. K. Jeong. Can shoulder muscle activity be evaluated with ultrasound shear wave elastography? *Clinical Orthopaedics and Related Research*, 476(6):1276, 2018.

T. K. Koo, J.-Y. Guo, J. H. Cohen, and K. J. Parker. Quantifying the passive stretching response of human tibialis anterior muscle using shear wave elastography. *Clinical Biomechanics*, 29(1):33–39, 2014.

H. Latorre-Ossa, J.-L. Gennisson, E. De Brosses, and M. Tanter. Quantitative imaging of nonlinear shear modulus by combining static elastography and shear wave elastography. *IEEE Transactions on Ultrasonics, Ferroelectrics, and Frequency Control*, 59(4):833–839, 2012.

G.-Y. Li and Y. Cao. Backward Mach cone of shear waves induced by a moving force in soft anisotropic materials. *Journal of the Mechanics and Physics of Solids*, 138: 103896, 2020.

G.-Y. Li, Y. Zheng, Y. Liu, M. Destrade, and Y. Cao. Elastic Cherenkov effects in transversely isotropic soft materials-i: theoretical analysis, simulations and inverse method. *Journal of the Mechanics and Physics of Solids*, 96:388–410, 2016.

R. G. Lopata, J. P. van Dijk, S. Pillen, M. M. Nillesen, H. Maas, J. M. Thijssen, D. F. Stegeman, and C. L. de Korte. Dynamic imaging of skeletal muscle contraction in three orthogonal directions. *Journal of Applied Physiology*, 109(3):906–915, 2010.

I. D. Loram, C. N. Maganaris, and M. Lakie. Use of ultrasound to make noninvasive in vivo measurement of continuous changes in human muscle contractile length. *Journal of Applied Physiology*, 100(4):1311–1323, 2006.

K. Miyatake, M. Yamagishi, N. Tanaka, M. Uematsu, N. Yamazaki, Y. Mine, A. Sano, and M. Hirama. New method for evaluating left ventricular wall motion by color-coded tissue doppler imaging: in vitro and in vivo studies. *Journal of the American College of Cardiology*, 25(3):717–724, 1995.

S. F. Nagueh, I. Mikati, H. A. Kopelen, K. J. Middleton, M. A. Quiñones, and W. A. Zoghbi. Doppler estimation of left ventricular filling pressure in sinus tachycardia: A new application of tissue doppler imaging. *Circulation*, 98(16):1644–1650, 1998.

A. Nordez and F. Hug. Muscle shear elastic modulus measured using supersonic shear imaging is highly related to muscle activity level. *Journal of Applied Physiology*, 108 (5):1389–1394, 2010.

A. Nordez, J. L. Gennisson, P. Casari, S. Catheline, and C. Cornu. Characterization of muscle belly elastic properties during passive stretching using transient elastography. *Journal of Biomechanics*, 41(10):2305–2311, 2008.

R. W. Ogden and B. Singh. Propagation of waves in an incompressible transversely isotropic elastic solid with initial stress: Biot revisited. *Journal of Mechanics of Materials and Structures*, 6(1):453–477, 2011.

C. F. Otesteanu, B. R. Chintada, M. B. Rominger, S. J. Sanabria, and O. Goksel. Spectral quantification of nonlinear elasticity using acoustoelasticity and shear-wave dispersion. *IEEE Transactions on Ultrasonics, Ferroelectrics, and Frequency Control*, 66(12):1845–1855, 2019.

S. Papazoglou, J. Rump, J. Braun, and I. Sack. Shear wave group velocity inversion in mr elastography of human skeletal muscle. *Magnetic Resonance in Medicine: An Official Journal of the International Society for Magnetic Resonance in Medicine*, 56 (3):489–497, 2006.

J. Petit, G. Filippi, F. Emonet-Denand, C. Hunt, and Y. Laporte. Changes in muscle stiffness produced by motor units of different types in peroneus longus muscle of cat. *Journal of Neurophysiology*, 63(1):190–197, 1990.

J.-Y. Reginster and N. Khaltaev. Introduction and WHO perspective on the global burden of musculoskeletal conditions. *Rheumatology*, 41(suppl_1):1–2, 2002.

N. C. Rouze, M. H. Wang, M. L. Palmeri, and K. R. Nightingale. Finite element modeling of impulsive excitation and shear wave propagation in an incompressible, transversely isotropic medium. *Journal of Biomechanics*, 46(16):2761–2768, 2013.

N. C. Rouze, M. L. Palmeri, and K. R. Nightingale. Tractable calculation of the Green's tensor for shear wave propagation in an incompressible, transversely isotropic material. *Physics in Medicine & Biology*, 65(1):015014, 2020.

A. P. Sarvazyan, O. V. Rudenko, S. D. Swanson, J. B. Fowlkes, and S. Y. Emelianov. Shear wave elasticity imaging: A new ultrasonic technology of medical diagnostics. *Ultrasound in Medicine & Biology*, 24(9):1419–1435, 1998.

K. Storheim and J.-A. Zwart. Musculoskeletal disorders and the global burden of disease study, 2014.

D. Tran, F. Podwojewski, P. Beillas, M. Otténio, D. Voirin, F. Turquier, and D. Mitton. Abdominal wall muscle elasticity and abdomen local stiffness on healthy volunteers during various physiological activities. *Journal of the Mechanical Behavior of Biomedical Materials*, 60:451–459, 2016.

T. Vos, A. D. Flaxman, M. Naghavi, R. Lozano, C. Michaud, M. Ezzati, K. Shibuya, J. A. Salomon, S. Abdalla, V. Aboyans, et al. Years lived with disability (ylds) for 1160 sequelae of 289 diseases and injuries 1990–2010: A systematic analysis for the Global Burden of Disease Study 2010. *The Lancet*, 380(9859):2163–2196, 2012.

WHO ScientificGroup. *The burden of musculoskeletal conditions at the start of the new millennium: Report of a WHO Scientific Group*, volume 919. World Health Organization, 2003.

A. D. Woolf and K. Åkesson. Understanding the burden of musculoskeletal conditions, 2001.

F. Yeung, S. F. Levinson, D. Fu, and K. J. Parker. Feature-adaptive motion tracking of ultrasound image sequences using a deformable mesh. *IEEE Transactions on Medical Imaging*, 17(6):945–956, 1998.